Three Dimensional Tetrapodal ZnO Microstructured Networks based Flexible Surface Acoustic Wave Device for Ultraviolet and Respiration Monitoring Applications

Xiang Tao,[†,‡] Hao Jin,[†,] Mona Mintken,[§] Niklas Wolff,[§] Yong Wang,[⁄⁄] Ran Tao,[‡] Yifan Li,[‡] Hamdi Torun,[‡] Jin Xie,[⁄⁄] Jingting Luo,[⊥] Jian Zhou,[#] Qiang Wu,[‡] Shurong Dong,[†] Jikui Luo,[†] Lorenz Kienle,[§] Rainer Adelung,[§] Yogendra Kumar Mishra,[ϕ,*] YongQing Fu[‡,⁄⁄,*]*

[†] College of Information Science and Electronic Engineering, Zhejiang University, Hangzhou 310027, China

[‡] Faculty of Engineering and Environment, Northumbria University, Newcastle upon Tyne, NE1 8ST, UK

[§] Institute for Materials Science, Kiel University, Kaiserstr. 2, D-24143, Kiel, Germany

[ϕ] Mads Clausen Institute, NanoSYD, University Southern Denmark, Alsion 2, 6400, Sønderborg, Denmark

// The State Key Laboratory of Fluid Power and Mechatronic Systems, Zhejiang University, Hangzhou 310027, China

⊥ Shenzhen Key Laboratory of Advanced Thin Films and Applications, College of Physics and Optoelectronic Engineering, Shenzhen University 518060, China

College of Mechanical and Vehicle Engineering, Hunan University, Changsha 410082, P. R. China

KEYWORDS: Flexible SAW sensor, ZnO tetrapods, Interconnected network, UV sensor, Humidity sensor

ABSTRACT: Sensitivity of flexible surface acoustic wave (SAW) sensors to ultraviolet (UV) light is enhanced by application of micro- and nano-structured ZnO networks as sensing layers. In this study, the influence of three dimensional (3D) tetrapodal ZnO microstructured networks spin coated onto Al foil/ZnO piezoelectric film SAW devices on the sensor performance under stimulus of UV light irradiation and influencs of relative humidity was investigated. The UV light sensitivity is increased from -3.03×10^{-6} cm^2mW^{-1} to -5.25×10^{-6} cm^2mW^{-1} with the application of 3D tetrapodal ZnO microstructured networks. Likewise, the humidity sensitivity is enhanced by a factor of 2.9 at 90% relative humidity, which is explained by the porous structure of tetrapodal ZnO microstructured networks. In addition, the measured sensitivity to UV light intensity is demonstrated to be significantly modified under a bent condition, because the surface of ZnO piezoelectric film is relatively denser in the case of bending. This study also demonstrates that the sensing performance of respiratory characteristics is increased by nearly a factor of 1.7 under bent

conditions after the utilization of the tetrapodal ZnO microstructured networks, showing it is capability for breath and respiration monitoring applications.

■ Introduction

Flexible surface acoustic wave (SAW) sensors are emerging in wearable applications, owing to their extreme sensitivity to mechanical, chemical, optical, electrical and biological stimuli on their surfaces [1–9]. Biological applications using SAW sensors have received much attention in recent years, because these sensors can be used to detect biomolecules through affinity binding with biomarkers for the detection of viruses, pathogens and early stage diagnosis of diseases [10]. Compared with other biological sensing technologies, such as optical fibre, surface plasmon resonance, and sensors based on field effect transistors or micro-cantilevers, the SAW sensors are advantageous as they offer high sensitivity, miniaturized size, low cost, outstanding accuracy, programmability and ease of use simultaneously [11,12]. Furthermore, the SAW sensors based on piezoelectric thin films and flexible substrates have great potential for implementation into integrated, disposable, bendable/flexible and wearable devices for sensing applications of temperature, humidity, heartbeat, pulse, etc [9,13].

There is a challenge to improve SAW sensors in terms of their sensitivity, response and recovery times, cost and ease of use [14]. One direction to address this challenge is to use layers of nano- and micro-structured networks with large surface-to-volume ratios and special physical/chemical properties [15,16] as highly sensitive functional layers [14,17,18]. For example, Xuan *et al.* [14] reported SAW humidity sensors based on ZnO piezoelectric film with graphene oxide (GO) as the performance-enhancing layer, which improved the sensitivity at a broad humidity

range from 0.5% RH to 85% RH with a response time shorter than 1 second. Jo *et al.* demonstrated a significant sensitivity improvement for their SAW ultraviolet (UV) sensor with a layer of UV-sensitive ZnO nanoparticles and another ultrathin gold layer [19]. Wang *et al.* reported highly sensitive hydrogen gas sensors using SnO_2 nanowires grown on Cd-Au comb-shape interdigitate electrodes, which were highly sensitive to a low concentration detection limit of 10 ppm [20]. Li *et al*. described a highly sensitive SAW UV detector using a sensing layer of ZnO nanorods (NRs) grown on ST-cut quartz using a hydrothermal method, which showed a higher UV light sensitivity than that based on the ZnO nano-film [21].

Although nano- and micro-structured networks are widely used to improve the sensitivity of sensors, they are generally complex and costly to synthesize [22–24]. This study utilizes flame transport synthesis (FTS) method to prepare unique tetrapodal ZnO micro- and nano-tetrapod interconnected network as a performance enhancing layer on the flexible SAW sensors [25]. The FTS method is a single-step process for direct conversion of Zn metallic particles into ZnO micro- and nano-tetrapods and can be easily extended to large scale synthesis in order to meet the industrial requirements [25–28]. The tetrapodal ZnO microstructured networks (T-ZnO MN) are extremely porous (up to 98%, density≈0.115 g/cm^{-3}) and stable [25,26], which can be used to increase the sensitivity of the flexible SAW humidity sensor as a sensitive layer. Moreover, the ZnO piezoelectric film and T-ZnO MN have an exciton binding energy of 60 meV, a large bandgap (E_g) of ~3.3 eV, so it is transparent in the visible wavelength range and has a superiority for UV radiation detection [18,19]. The T-ZnO MN with large surface-to-volume ratios also enables high spectral selectivity and UV sensitivity [29]. The highly porous T-ZNO MN could be beneficial for humidity, breathe, or respiration monitoring applications.

In the present work, we fabricated flexible SAW sensors with different wavelengths based on ZnO piezoelectric film on aluminium (Al) foil substrates. The flexural wave mode based SAW device with a wavelength of 100 μm was chosen for T-ZnO MN modification. The T-ZnO MN was spun coated onto the surface of flexible SAW sensor as the performance-enhancement layer. The enhanced effect of the T-ZnO MN on the UV performance has been investigated in detail, in both flat and bending modes, and we also demonstrated the humidity and respiratory monitoring capabilities using the flexible SAW sensors with T-ZnO MN layer.

■ Experimental Section

The designed structure of the flexible SAW sensor coated with T-ZnO MN is illustrated in Figure 1(a), and the photograph of the sensor is shown in Figure S1 in the Supporting Information. The ZnO piezoelectric film with a thickness of 5.5 μm was deposited onto an Al foil with a thickness of 50 μm using a conventional DC magnetron sputter. The interdigitated transducers (IDTs) were formed on a 150 nm-thick sputtered Al film using a standard lift-off process. The detailed production process is shown in Figure S2. The wavelengths of the flexible SAW sensors on Al foils were designed to be 32 μm, 100 μm and 400 μm, and the wave modes were characterized using a network analyser (HP8752A).

The preparation process for 3D T-ZnO MNs using the FTS technique was reported previously [25,28,30,31]. In a standard FTS process, a mixture of Zn particles (with an average diameter of 5 mm, from GoodFellow, UK) and poly(vinyl butyral) (PVB) powder (Mowital B 60H from Kuraray GmbH, Europe) with a weight ratio of 1:2 was placed in a ceramic crucible and then heated to 900 °C in a muffle furnace [26,28,30,32,33]. The PVB polymer mainly plays the

role of sacrificial layer which is decomposed at a high temperature in the heating process in the furnace. During the burning, the Zn microparticles are converted into Zn atomic vapour which, with help from native oxygen molecules, participates in standard nucleation and growth processes to form T-ZnO micro and nanostructures via a solid-vapour-solid growth mechanism. [25]. A variation of the process involved heating Zn powder under a nitrogen atmosphere instead of using a sacrificial polymer until the reaction temperature was reached [25–27], thus leading to the growth of fluffy T-ZnO micro- and nanostructured network with higher aspect ratios of each arms.

The T-ZnO microstructure solution was prepared by dissolving the ZnO tetrapodal structures in absolute ethyl alcohol with a concentration of 0.01 g/cm^3. The ZnO microstructure solution was spin-coated onto the surface of flexible SAW sensor at 500 rpm for 10 s to spread the solutions, and the as-coated ZnO microstructured sensing layer was dried overnight in air at room temperature, and the layer thickness was ~30 μm. The morphological studies on these ZnO tetrapods were carried out using a scanning electron microscope (SEM, Ultra 55 Zeiss FEG at 7 kV). The ZnO tetrapods were analysed with respect to their crystal structures using a high-resolution X-ray diffractometer (XRD, Siemens D5000) operated at 40 kV and 10 μA ($CuK\alpha_1$ radiation with λ=1.5406 Å) and transmission electron microscopy (TEM, Tecnai F30). A Raman spectroscope (WITec Alpha300 RA spectrometer in backscattering configuration interfaced with a digital photometer and data acquisition processor) was used with a Nd-YAG laser (532 nm line).

The experimental apparatus for flexible SAW UV sensor with the T-ZnO MN is schematically illustrated in Figure 1(b), which was connected to a network analyser to record the

frequency data. Different intensities of UV light were generated using a UV gun (CS2010, Thorlabs Inc, USA) and then irradiated onto the SAW UV sensor with an area of 1.2 cm in diameter. The wavelength of the UV source was 365 nm. A LabVIEW (National Instruments Inc.) based program was developed to implement real-time measurements of frequency changes of the flexible SAW UV sensors.

Humidity monitoring using the flexible SAW sensor was performed unsing a home-made measurement system which was reported in our previous paper [34]. The humidity values were changed from 30% RH to 90% RH, and the frequency data were continuously recorded using a LabVIEW-based data acquisition and control system. We have also employed the flexible SAW sensor to detect and monitor respiration as a case study based on its sensitivity for the changes in humidity and temperature. The flexible SAW sensor with a wavelength of 100 μm was used for this experiment where we bonded it onto a small Flexible Printed Circuit (FPC), and attached the FPC on the upper lip of a volunteer. The sensor was bent to conform the shape of the individual's upper lip. The resonant frequency of the sensor was recorded while the volunteer was breathing continuously.

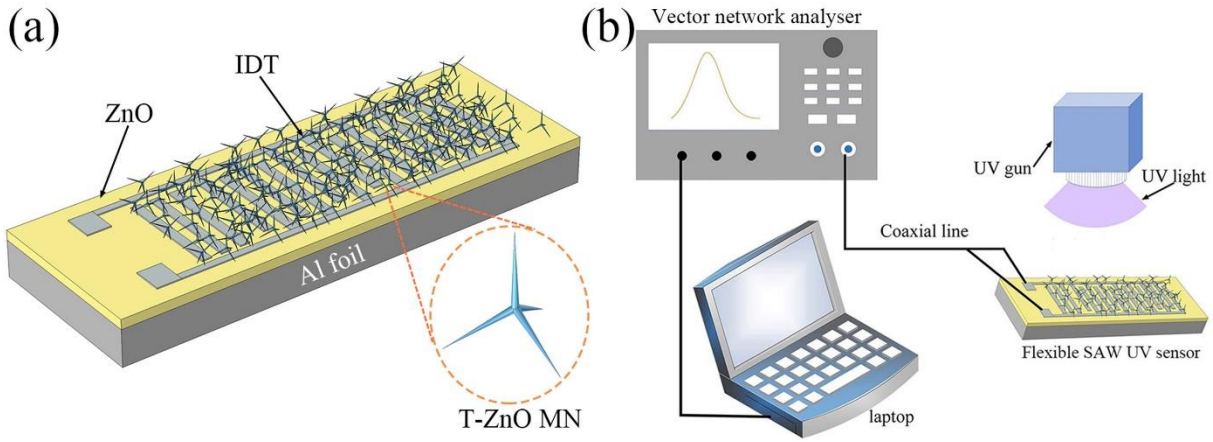

Figure 1. (a) Flexible SAW sensor with T-ZnO MN, (b) experimental apparatus for analysing the sensing properties of the flexible SAW UV sensor with T-ZnO MN.

■ Results and discussion

Characterisation of T-ZnO MN

A typical SEM image of T-ZnO MN, which was used to build the sensing layer, is shown in Figure 2(a), with an inset figure showing a photograph of the synthesized T-ZnO powders inside a glass beaker. The average diameter of the T-ZnO microstructures is about 20.3 μm, and the diameter of the arms (defined as the diameter at half the length of the arm) is about 250 nm. The size of T-ZnO microstructures is mainly affected by the metal-polymer ratio and temperature profile in the furnace. In addition, the location inside the furnace also matters, as there are small variations in size and shape depending on the location from which they were harvested [25]. Each tetrapod consists of four arms converging in a central core at angles between ~105 ° and 110 °, cf. Figure 2(a). This shape combines the properties of 1D ZnO nanorods or needles, forming highly porous interconnected network with plenty of bridging junctions [25,26]. The tetrapodal shape of these structures is effective in constructing the flexible and structurally intact mechanically-stable 3D networks with a high porosity and a large surface-to-volume ratio, enhancing the sensing performance of the flexible SAW sensors [26].

X-ray diffractogram corresponding to T-ZnO nano- and micro-structured network is shown in Figure 2(b) and all the observed reflections can be assigned to wurtzite type ZnO (JCPDS Card-36-1451). The prominent reflections, e.g., (10-10), (0002) and (10-11), are corresponding to the wurtzite ZnO phase, indicating highly crystalline nature of the synthesized ZnO tetrapods after the FTS process. The Raman spectrum of the T-ZnO MN is shown in Figure 2(c). For the

wurtzite ZnO, there are 12 degrees of freedom since there are 4 atoms per primitive cell [27,35]. In group theory, $\Gamma_{opt} = A_1(z) + 2B_1 + E_1(x, y) + 2E_2$, where x, y, and z represent the polarization directions [36]. The A_1, E_1 and E_2 modes are Raman-active, and the A_1, E_1 modes are also infrared active, polar, and split into transverse optical (TO) and longitudinal optical (LO) components [22,36,37]. The lower-frequency E_2 (low) mode in T-ZnO MN is associated with the vibration of heavy Zn sub-lattice [22]. The higher-frequency E_2 (high) mode is a characteristic of the wurtzite phase, which involves only the oxygen atoms [35]. The B_1 mode is IR- and Raman-inactive mode, or silent mode [36].

Figures 2(d-g) show the TEM image of the ZnO tetrapods. The ZnO tetrapods consist of single and adnate tetrapods of various dimensions as shown in Figure 2(d). It should be noted that only the thin parts of small tetrapods and tetrapod arms can be transmitted with the electron beam. For demonstrating the c-axis directed growth of the ZnO tetrapod arms (Figure 2(e)) in the wurtzite-type crystal structure, a high-resolution TEM image (Figure 2(f)) and its corresponding electron diffraction pattern (Figure 2(g)) were obtained. Results show ZnO tetrapad grows along the (0001) lattice planes, which is resembled in the [10-10] zone axis pattern.

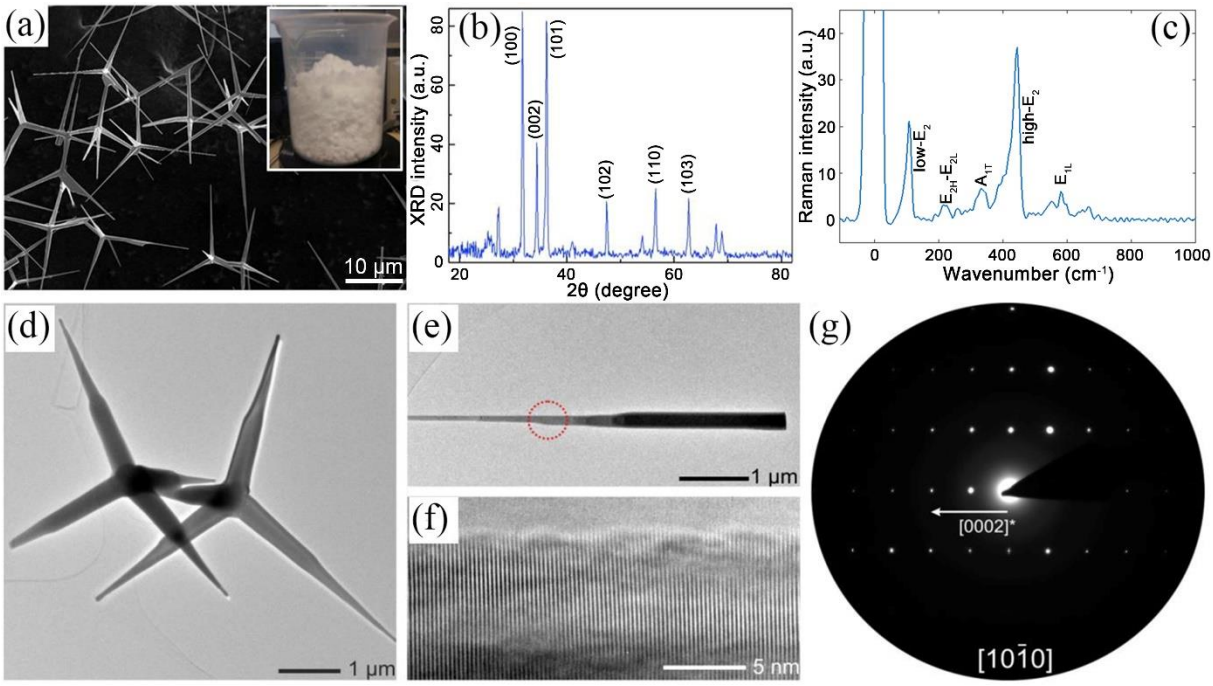

Figure 2. (a) SEM image of ZnO micro and nanostructures showing their tetrapodal morphology. (b) XRD pattern and (c) micro-Raman spectrum of the ZnO tetrapods. (d) Low-magnification TEM images of adnate ZnO tetrapods from a tetrapod network and (e) one broken-off tetrapod arm. (f) High-resolution TEM image showing the (0001) lattice planes of ZnO perpendicular to the growth direction of the crystal. (g) Electron diffraction pattern in [10-10] zone axis orientation of the wurtzite-type crystal structure.

Characterization of flexible SAW sensors

Reflection spectra (S_{11}) of one-port flexible SAW sensors with different wavelengths are shown in Figure 3(a). Clearly, the S_{11} peaks are determined by the wavelength, and all the resonant peaks of the flexible SAW sensors are listed in Table S1 in the Supporting Information. The S_{11} spectrum of the flexible SAW sensor with the T-ZnO MN is also shown in Figure 3(a).

The frequency of each resonant peak is slightly decreased after applying the T-ZnO MN indicating the effect of mass loading. When the wavelength of the sensor is smaller than the thickness of the substrate, the resonance peak is from the Rayleigh wave (e.g., 32 μm wavelength). Lamb waves are generated when the substrate thickness is smaller than or comparable to the wavelength of the acoustic wave (e.g., 100 μm and 400 μm wavelengths). There are multiple wave modes (with different frequencies in S_{11} results) for the flexible SAW devices with wavelengths of 100 μm and 400 μm. Finite-element method-based simulations using COMSOL software were used to verify the vibration modes of resonant peaks. A simplified 3D-model with ideal material parameters, e.g., one pair of IDTs electrode and periodic boundary conditions, were used to simulate flexible SAW devices with different wavelengths. The thicknesses of Al foil layer, ZnO piezoelectric thin film and electrode layer were set to be 50 μm, 5.5 μm and 0.15 μm, respectively. The finger aperture was designed as one-wavelength wide. The boundary of the left terminal was set to be electrical ground, and that of the right terminal was assigned to the floating potential with zero surface charge accumulation. This combination of electrical boundary conditions corresponds to an open circuit configuration, which is suitable for sensing applications.

Figure 3(b) is the total displacement diagram of the first resonant peak of the flexible SAW sensor with a wavelength of 100 μm, and it is a typical zero-order asymmetric Lamb mode (A_0). From the COMSOL simulation, we observe Lamb waves as the dominant mode for the device with wavelengths of 100 μm and 400 μm, whereas the dominant wave mode is Rayleigh waves for the device with a wavelength of 32 μm. Figures 3(c) and 3(d) show the typical zero-order symmetrical Lamb wave mode (S_0) for the wavelength of 100 μm, and Rayleigh wave mode for the device with wavelength of 32 μm.

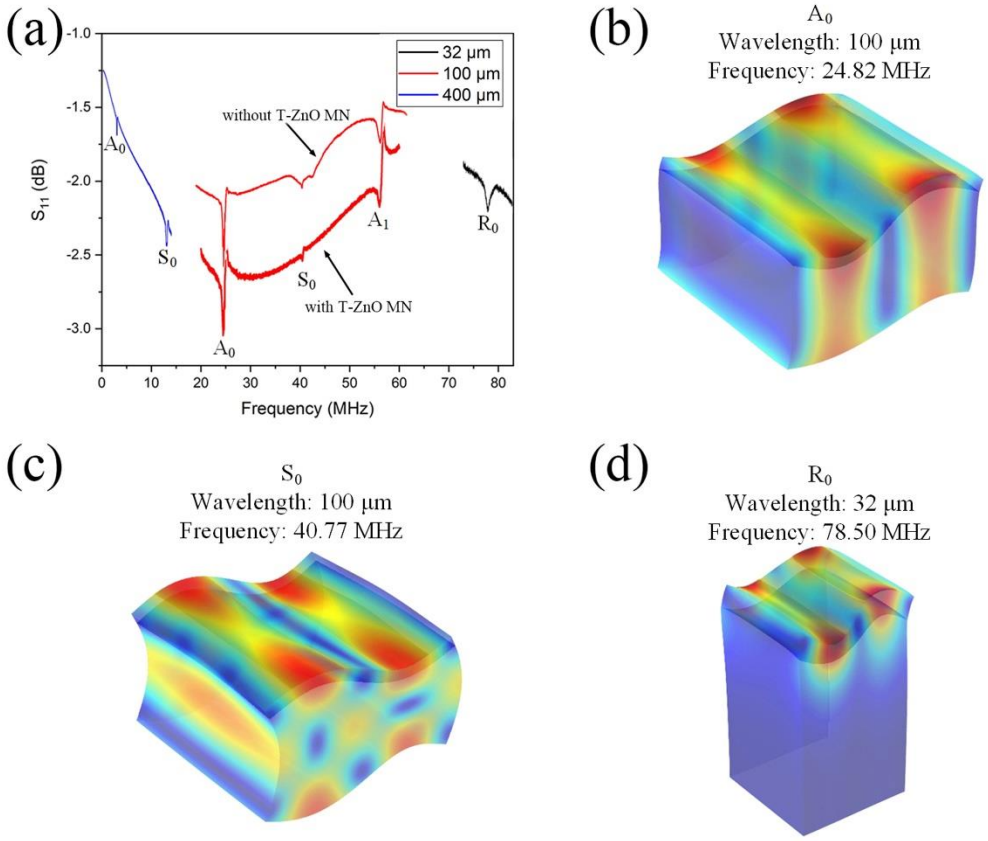

Figure 3. (a) The reflection spectrum of the flexible SAW sensor with T-ZnO MN, the total displacement diagram of (b) the A_0 mode (100 μm wavelength), (c) the S_0 mode (100 μm wavelength) and (d) the R_0 mode (32 μm wave-length).

Sensing characterisations

UV detection using flexible SAW sensor without T-ZnO MN coating

The UV responses of various vibration modes of flexible SAW sensors with different wavelengths were tested, and a typical UV response of flexible SAW sensors without using the

T-ZnO MN is shown in Figure 4(a). The wavelength of the flexible SAW sensor is 100 μm, and the vibration mode is A_0. When the device is exposed to UV light, the resonant frequency of the flexible SAW sensor is decreased due to the generation of excess carriers in ZnO, thus resulting in the increased capacitance [38]. This effect is reversible with resonant frequency recovering to its original value when the UV excitation is switched off. The UV sensitivity of the flexible SAW sensor can be defined by the following formula [39]:

$$S = \frac{\Delta f}{f_0 \Delta I_{UV}} \qquad (1)$$

where S is the sensitivity, f_0 is the original resonant frequency, Δf is the frequency shift, and ΔI_{UV} is the UV intensity. The normalized frequency shifts ($\Delta f / f_0$) of various vibration modes under different UV intensities are shown in Figure 4(b), and the slopes of various curves are the UV sensitivities of vibration modes, which are summarised in Table 1.

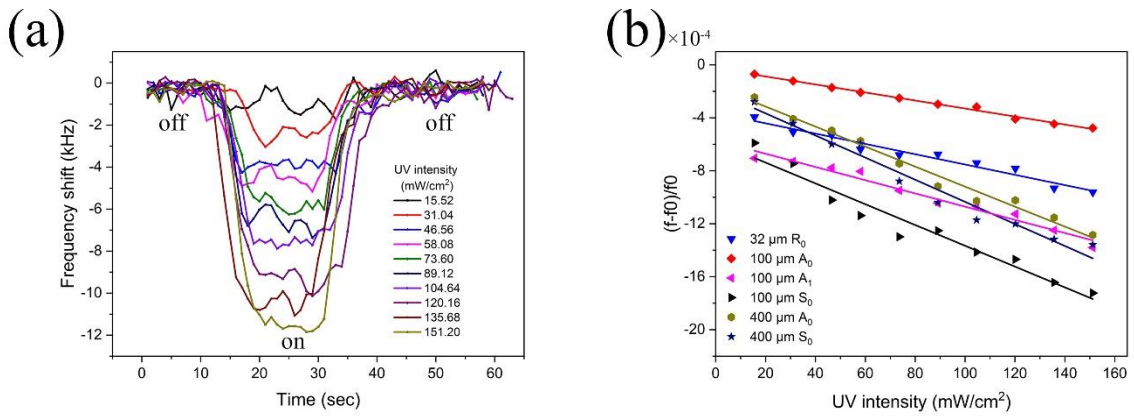

Figure 4. (a) UV response of flexible SAW sensors (100 μm wavelength, A_0 mode) without T-ZnO MN, (b) The nor-malized frequency shifts of various vibration modes under different UV intensities.

The shift in resonant frequency of flexible SAW sensors upon UV irradiation is attributed to two factors: 1) surface oxygen-adsorbed species [18]; 2) thermal effect, as the UV source will also induce heating. The absorbed oxygen molecules on the surface of the ZnO piezoelectric thin film and T-ZnO MN capture the free electrons [$O_2(g) \leftrightarrow O_2(ad), O_2(ad) + e^- \rightarrow O_2^-(ad)$], and create a low-conductivity depletion region at atmospheric conditions without UV excitation [40]. The surface adsorbed oxygen molecules capture the photo-generated holes [$O_2^-(ad) + h^+ \rightarrow O_2(g)$] when the UV excitation is switched on [19], thus narrowing the depletion region and drastically enhancing the overall conductivity in the ZnO piezoelectric thin film and T-ZnO MN. The change in conductivity results in a change in the resonant frequency of the flexible SAW sensor, which is given by [41]:

$$\Delta f_\sigma = \frac{f_0 K^2}{2} * \frac{1}{1+\left(\frac{v_0 c_s}{\sigma}\right)^2}, \quad c_s = \varepsilon_0 + \varepsilon_s \qquad (2)$$

where Δf_σ is the frequency shift caused by conductivity change, σ is the sheet conductivity of the ZnO, ε_0 and ε_s are air and substrate dielectric permittivities, respectively, and K^2 is the electromechanical coupling coefficient of the substrate. The electromechanical coupling coefficients of the flexible SAW sensor was obtained using the following formula [6,37,42]:

$$K^2 = \frac{\pi}{4N}\left(\frac{G}{B}\right)_{f=f_0} \qquad (3)$$

where *N* is the number of the finger pairs, G and B are the radiation conductance and susceptance at the original resonant frequency, respectively.

In addition, UV light will change the surface temperature of the surface of flexible SAW sensor, causing frequency shifts. The frequency shift induced by the temperature change is given by [43]:

$$\Delta f_T = f_0 * TCF * \Delta T \quad (4)$$

where Δf_T is the frequency shift caused by temperature change, *TCF* is the temperature coefficient of frequency of flexible SAW sensor, and ΔT is change of the temperature. The *TCF* values were obtained by recording the frequency shifts of the flexible SAW sensor which was put inside an oven (with a temperature variation ranging from room temperature up to 80 ºC and a resolution of 0.1 ºC), and then calculating the linear slopes of the frequency shift vs temperature. The details of the *TCF* results are listed in Table S1 in the Supporting Information. The obtained results of frequency, UV sensitivity, *TCF* and K^2 of different flexible SAW sensors are listed in Table 1 for comparisons.

Table 1. The frequency, UV sensitivity and *TCF* of different flexible SAW sensors

Wavelength and mode	Frequency (MHz)	Sensitivity (slope)	*TCF* (ppm/º C)
400 μm S_0	12.53	-8.35×10^{-6}	-539.1
400 μm A_0	2.79	-7.85×10^{-6}	-459.8
100 μm S_0	40.77	-7.55×10^{-6}	-330.2
100 μm A_1	56.74	-4.99×10^{-6}	-270.2
32 μm R_0	78.48	-3.89×10^{-6}	-243.1
100 μm A_0	24.80	-3.03×10^{-6}	-205.3

From Table 1, it can be seen that there is no clear indication of the dependence of the sensitivity upon the overall frequency values of all the sensors, but for the same group of Lamb wave devices, the sensitivity seems decreasing with the increase of device's frequencies. However, detailed analysis of the data showed that the larger the *TCF*, the higher the UV sensitivity of the wave mode. Therefore, the effect of temperature changes on the UV response of flexible SAW sensor should not be ignored.

UV detection using flexible SAW sensor with different bending angles

The flexible SAW sensors based on Al foils have good flexibility, and can be bent freely within a certain range. The device still can be used to monitor the frequency signals even after being fully folded. More details about flexibility of the flexible devices can be found from our previous paper [13]. They can be fitted onto non-flat or complex surfaces of an object, which shows great application prospects in wearable and flexible personal electronics. The flexible SAW sensor with a wavelength of 400 μm was bent into different angles (Figure 5(a)), and the stain of flexible SAW sensor under each bending angle was calculated. The relationship between strain and resonant frequency of the flexible SAW sensor is shown in Figure 5(b). Clearly, the resonant frequency is increased as the strain is increased, and the increasing trend is decreased when the strain is larger than 600 με. We have examined the bending fatigue/deformation reproducibility performance of the related devices in our previous paper [13], and the flexible SAW device was bent for 2000 cycles at a fixed strain. The frequency and amplitude were decreased rapidly in the first 500 cycles; however, they became stable after 500 cycles. There are some cracks on film surface of the device after repeated bending test, but the SAW device still showed good

performance, mainly because the acoustic wave mode was flexural Lamb wave mode [13]. The frequency shifts of flexible SAW sensors with strains of 0 and 600 με are shown in Figure 5(c), and the normalized frequency shifts are shown in Figure 5(d) for comparisons. It can be seen from Figures 5(c) and 5(d), the UV response of bent SAW sensor with strain of 600 με is better than that of flat SAW sensor with strain of 0 με, and the UV sensitivity of flexible SAW sensor has also almost doubled under the bending condition. The UV sensitivities of flexible SAW sensors with strains of 0 με and 600 με are -7.85×10^{-6} cm^2mW^{-1} and -1.53×10^{-5} cm^2mW^{-1}, respectively.

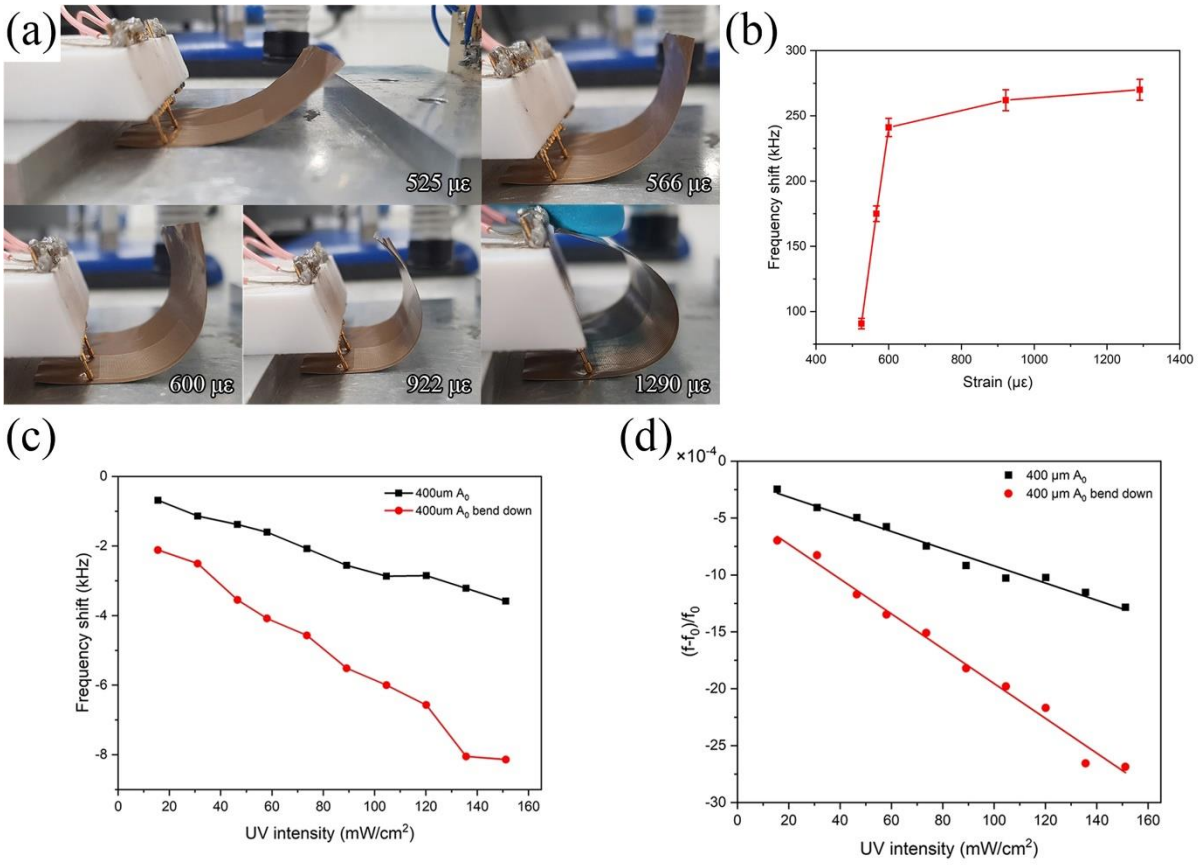

Figure 5. (a) Photographs of flexible SAW sensor with a wavelength of 400 μm under different bending positions, (b) the relationship between stain and resonant frequency of the flexible SAW sensor, (c) the frequency shifts and (d) the normalized frequency shifts of flexible SAW sensors with strains of 0 με and 600 με.

UV detection using flexible SAW sensor coated with T-ZnO MN layer

In the following experiments, the A_0 mode device (100 μm wavelength) was selected for UV, humidity and respiratory sensing, because it has minimised temperature effects. We also calculated the frequency shifts caused by temperature effect according to Eq. 4, and the temperature changes of the flexible SAW sensors during UV process were estimated using a thermocouple. The UV responses of flexible SAW sensors with a layer of T-ZnO MN are shown in Figure 6(a). As previously analysed, the highly porous T-ZnO MN layer will increase the oxygen molecules absorbed on the surface of the SAW sensor, which will enhance the overall conductivity under UV light illumination. Therefore, the frequency shift of flexible SAW sensor coated with the T-ZnO MN (Figure 6(a)) is much larger than the flexible SAW sensor without the T-ZnO MN (Figure 4(a)). The frequency shifts of flexible SAW sensors without/with T-ZnO MN layer under different UV intensities are shown in Figure 6(b) for comparisons. The frequency shifts of both flexible SAW sensors are increased with the increase of UV intensity, with a good linearity. Noticeably, the frequency shift of the flexible SAW sensor has almost been doubled after using the sensitive layer of T-ZnO MN. The normalized frequency shifts ($\Delta f/f_0$) under different UV intensities are shown in Figure 6(c), and the UV sensitivities are -3.03×10^{-6}

cm^2mW^{-1} and -5.25×10^{-6} cm^2mW^{-1}, respectively. Clearly, adding the layer of T-ZnO MN has significantly enhanced the UV sensitivity of the SAW sensor.

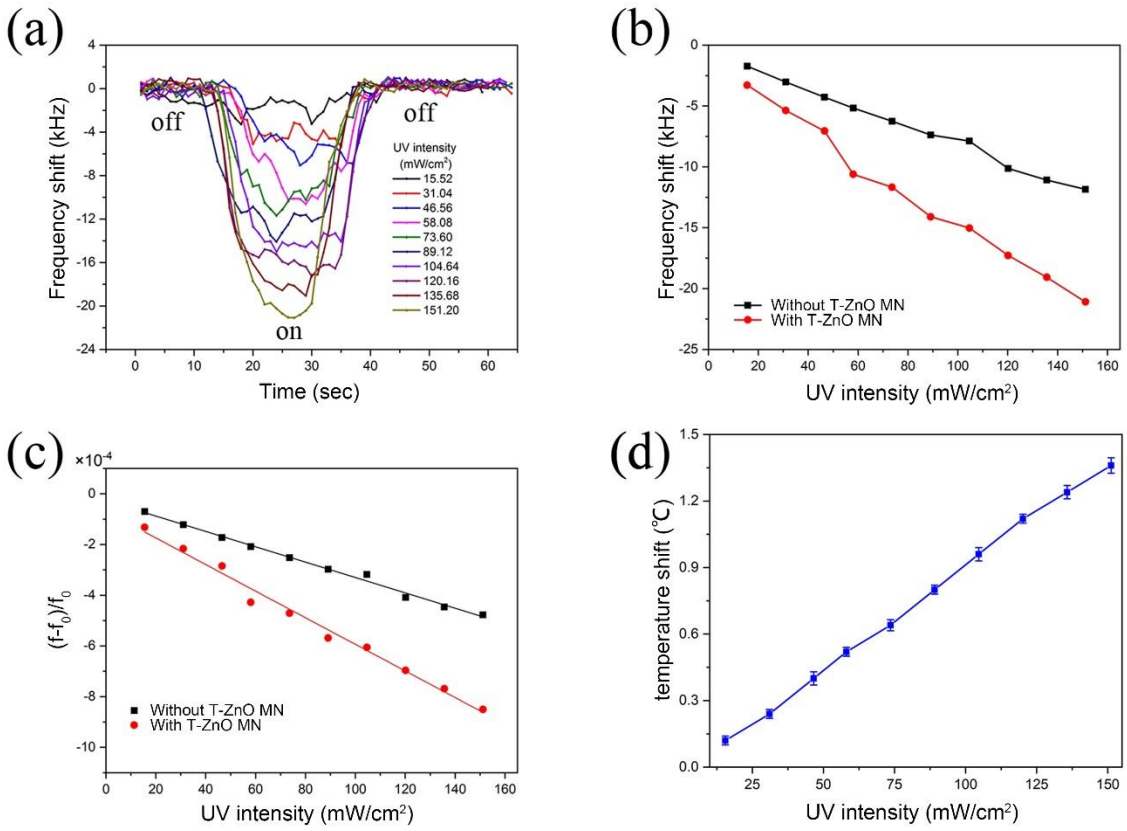

Figure 6. (a) The UV responses of flexible SAW sensors with T-ZnO MN, (b) the frequency shifts, (c) the normalized frequency shifts and (d) the temperature shift of two kinds flexible SAW sensors under different UV intensities.

In order to investigate the effects of temperature and conductivity on the UV responses of flexible SAW sensors, we tested the changes of surface temperature (Figure 6(d)) and

conductance (Figures 7(a) and 7(b)) of the flexible SAW sensors under different UV intensities. It can be seen from Figure 6(d), the temperature is increased linearly with the increase of UV intensity. The *TCF* value of the flexible SAW sensor is unchanged after using T-ZnO MN, therefore, the Δf_T of flexible SAW sensor without/with T-ZnO MN are almost the same based on Eq. 4.

The I-V characteristics of flexible SAW sensors without/with T-ZnO MN modification under different UV intensities are shown in Figures 7(a) and 7(b), respectively. When the UV light is irradiated on the device, the conductivity (i.e., the slope of I-V curve) of the flexible SAW sensor increases. The conductivity increases with the UV intensity, and the T-ZnO MN enhances this effect by a factor of 10^3. Based on the Eqs. 2 and 4, the theoretical frequency shifts caused by conductivity change (Δf_σ) and temperature change (Δf_T) can be obtained, respectively. The results are summarized in Figures 7(c) and 7(d). The theoretical ($\Delta f_\sigma + \Delta f_T$) and measured results of these flexible SAW sensors are also shown in Figures 7(c) and 7(d). The Δf_T values of two types of flexible SAW sensors are almost the same, while the Δf_σ is significantly increased after using T-ZnO MN layer. Therefore, the key mechanism of using T-ZnO MN layer to improve the UV sensitivity is the increase in conductivity under the UV light illumination. The experimental results of flexible SAW sensor without T-ZnO MN are in a good agreement with the theoretical result, while those of flexible SAW sensor with T-ZnO MN sensing layer is slightly deviating, possibly due to the presence of defects in the T-ZnO MN layer.

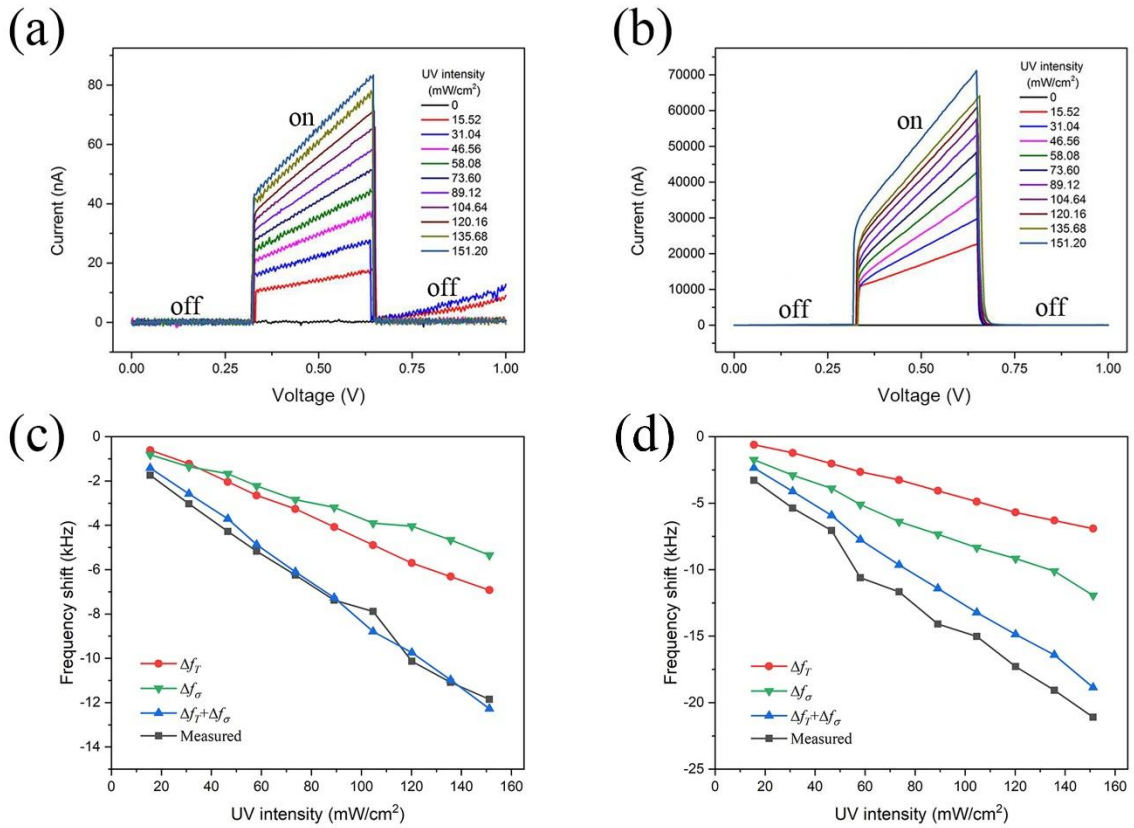

Figure 7. The I-V characteristic curve of flexible SAW sensors (a) without T-ZnO MN, (b) with T-ZnO MN under different UV intensities, the theoretical and measured results of flexible SAW sensors (c) without T-ZnO MN, (d) with T-ZnO MN under different UV intensities.

Humidity and respiration detection for flexibility demonstrations

The humidity responses of flexible SAW sensors without/with T-ZnO MN layers are shown in Figure 8(a). It can be seen from Figure 8(a) that the resonant frequency of flexible SAW sensors is decreased parabolically with relative humidity, and the T-ZnO MN enhances the frequency shifts. In general, the higher the relative humidity, the larger the difference in frequency shifts between two types of flexible SAW sensors. When the relative humidity is 90%

RH, the frequency shifts of flexible SAW sensor without/with T-ZnO MN are 9.66 kHz and 28.02 kHz, respectively.

We have further employed the flexible SAW sensor to detect and monitor respiration as a case study based on its sensitivity for the changes in humidity and temperature [1]. The resonant frequencies of flexible SAW sensors without/with T-ZnO MN under continuous and uniformly respirations as a function of time are shown in Figure 8(b). The resonant frequency of flexible SAW sensors is shifted downwards when the volunteer exhales due to the change in temperature and humidity, and the resonant frequency is increased when the volunteer inhales, but the overall frequency drifts downwards with time. It can be seen from Figure 8(b), the resonant frequency shifts of the flexible SAW sensors without/with T-ZnO MN caused by expiratory air are about 45.55 kHz and 66.33 kHz, respectively.

The temperature and relative humidity of the laboratory were recorded during the experiment as ~20 °C and ~38% RH, respectively. In addition, a thermocouple was used to measure the temperature of the flexible SAW sensor during the experiment. Results show that the temperature was increased up to ~7° due to the expiratory air. The frequency shifts due to the temperature changes can be calculated using Eq. 4 and the calculated value is 35.64 kHz. The relative humidity of exhaled air was also measured using a reference sensor (SHT71) and the reading was ~92.3% RH. It can be seen from Figure 8(a) that when the relative humidity is changed from 38% RH to 90% RH, the resonant frequency of the flexible SAW sensor without T-ZnO MN is decreased by 9.52 kHz, while that of the flexible SAW sensor with T-ZnO MN is decreased by 27.51 kHz. Therefore, the total frequency shifts caused by temperature and humidity changes for these two kinds flexible SAW sensors are 45.16 kHz and 63.15 kHz, which are in good agreements with the test results (45.55kHz and 66.33kHz respectively). It can be

concluded that the main reason for the frequency shift for these two flexible SAW sensors during the respiration is the temperature change. When the ambient temperature is close to the temperature of exhaled air, the humidity change can still be used for respiratory detection, which highlights the wider applicability of the flexible SAW sensor.

We can further obtain the information such as respiratory rate and respiratory intensity by monitoring the resonant frequency of the flexible SAW sensor, and the results are shown in Figure 8(b). The ZnO thin film is polycrystalline in nature, capable of absorbing water molecules inside. The releasing time frame of absorbed water is much longer than the period of inhaling, explaining the overall decrease in the resonant frequency with time [1]. Nevertheless, the frequency shift of the flexible SAW sensor has been nearly doubled after using the T-ZnO MN layer, proving that the T-ZnO MN layer has a significantly enhanced sensitivity for the flexible SAW sensor on respiratory detection, due to its higher sensitivity to both the humidity and temperature in comparison with the original flexible SAW sensor without this layer.

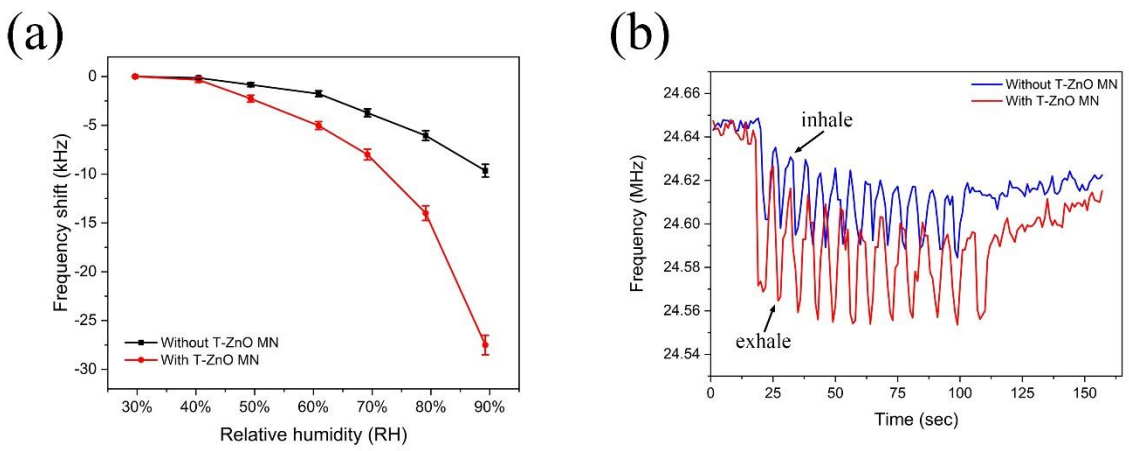

Figure 8. (a) The humidity responses of flexible SAW sensors without/with T-ZnO MN, (b) the resonant frequencies of flexible SAW sensors without/with T-ZnO MN under continuous, uniformly respiration.

■ Conclusions

In summary, a highly porous T-ZnO MN layer was synthesized and utilized as a performance enhancing sensing layer for flexible SAW UV sensor. This 3D T-ZnO MN layer offers excellent properties for sensing applications, mainly being highly porous and providing high surface-to-volume ratios. In present work, we fabricated flexible SAW UV sensors with different wavelengths based on ZnO piezoelectric films on Al foil substrates. The T-ZnO MN-applied flexible SAW sensors were used for UV and humidity sensing as well as respiration monitoring. The A_0 mode (with 100 μm wavelength IDTs) was used for the experiments. Results revealed an increase in UV sensitivity from -3.03×10^{-6} cm^2mW^{-1} to -5.25×10^{-6} cm^2mW^{-1} with the application of T-ZnO MN layer. Likewise, the humidity sensitivity is increased by 2.9 times at 90% RH, and the respiratory sensitivity is increased by 1.7 times. The investigations of this study suggest that such a flexible SAW sensor coated with T-ZnO nano- and microstructured network could be easily mass produced and efficiently utilized for UV, humidity and breathe/respiration monitoring applications in future technologies.

ASSOCIATED CONTENT

Supporting Information.

The Supporting Information is available free of charge via the Internet at http://pubs.acs.org. The photograph of the flexible SAW sensor coated with T-ZnO MN is shown in Figure S1. The detailed production process of flexible SAW sensor coated with T-ZnO MN is shown in Figure S2. The detail *TCF* results of various vibration modes are listed in Table S1.

AUTHOR INFORMATION

Corresponding Author

* E-mail: hjin@zju.edu.cn (H.J.)

* E-mail: richard.fu@northumbria.ac.uk (Y.Q.F.)

* E-mail: mishra@mci.sdu.dk (Y.K.M.)

Author Contributions

The manuscript was written through contributions of all authors. All authors have given approval to the final version of the manuscript.

Notes

The authors declare no competing financial interest.

ACKNOWLEDGMENT

This work was supported by the National Key R&D Program of China [grant number 2018YFB2002500]; the UK Engineering and Physical Sciences Research Council (EPSRC) [grant number EP/P018998/1]; Special Interest Group of Acoustofluidics from UK Fluids Network, Newton Mobility [grant number IE161019] through Royal Society; Zhejiang Lab

[grant number 2018EB0ZX01]; the Zhejiang Province Key R & D programs [grant number 2018C01037]; the Zhejiang Provincial Public Technology Research and Social Development Project [grant number LGF19F010007]; German Research Foundation under the schemes SFB 1261, TP [grant numbers (A05, RA), (A06, LK)]; National Natural Science Foundation of China [grant number 51605485]; Hunan Provincial Key R&D Program [grant number 2019GK2111]; Zhejiang University Education Foundation Global Partnership Fund.

ABBREVIATIONS

SAW, surface acoustic wave; UV, ultraviolet; FTS, flame transport synthesis; T-ZnO MN, tetrapodal ZnO microstructured networks; IDTs, interdigitated transducers; FPC, Flexible Printed Circuit; S_{11}, Reflection spectra; A_0, zero-order asymmetric Lamb mode; S_0, Lamb wave mode.

REFERENCES

(1) Jin, H.; Tao, X.; Dong, S.; Qin, Y.; Yu, L.; Luo, J.; Deen, M. J. Flexible Surface Acoustic Wave Respiration Sensor for Monitoring Obstructive Sleep Apnea Syndrome. *J. Micromechanics Microengineering* **2017**, *27* (11), 115006.

(2) Preethichandra, D. M. G.; Kaneto, K. SAW Sensor Network Fabricated on a Polyvinylidine Difluoride (PVDF) Substrate for Dynamic Surface Profile Sensing. *IEEE Sens. J.* **2007**, *7* (5), 646–649.

(3) He, X. L.; Li, D. J.; Zhou, J.; Wang, W. B.; Xuan, W. P.; Dong, S. R.; Jin, H.; Luo, J. K. High Sensitivity Humidity Sensors Using Flexible Surface Acoustic Wave Devices Made on Nanocrystalline ZnO/Polyimide Substrates. *J. Mater. Chem. C* **2013**, *1* (39), 6210–6215.

(4) Tricoli, A.; Nasiri, N.; De, S. Wearable and Miniaturized Sensor Technologies for Personalized and Preventive Medicine. *Adv. Funct. Mater.* **2017**, *27* (15), 1605271.

(5) Wang, Y.; Zhi, Y.; Hou, Z.; Dong, X.; Wei, L.; Kong, S. W.; Zhang, Y. Flexible Gas Sensors with Assembled Carbon Nanotube Thin Films for DMMP Vapor Detection. *Sensors Actuators B Chem.* **2010**, *150* (2), 708–714.

(6) Fu, Y. Q.; Luo, J. K.; Nguyen, N. T.; Walton, A. J.; Flewitt, A. J.; Zu, X. .; Li, Y.; McHale, G.; Matthews, A.; Iborra, E.; Du, H.; Milne, W. I. Advances in Piezoelectric Thin Films for Acoustic Biosensors, Acoustofluidics and Lab-on-Chip Applications. *Prog. Mater. Sci.* **2017**, *89*, 31–91. https://doi.org/10.1016/J.PMATSCI.2017.04.006.

(7) Grate, J. W.; Martin, S. J.; White, R. M. Acoustic Wave Microsensors. *Anal. Chem.* **1993**, *65:21* (21).

(8) Jo, M. C.; Guldiken, R. Particle Manipulation by Phase-Shifting of Surface Acoustic Waves. *Sensors Actuators A Phys.* **2014**, *207* (1), 39–42.

(9) He, X.; Guo, H.; Chen, J.; Wang, W.; Xuan, W.; Xu, Y.; Luo, J. Bendable ZnO Thin Film Surface Acoustic Wave Devices on Polyethylene Terephthalate Substrate. *Appl. Phys. Lett.* **2014**, *104* (21), 213504. https://doi.org/10.1063/1.4879850.

(10) Länge, K.; Rapp, B. E.; Rapp, M. Surface Acoustic Wave Biosensors: A Review. *Anal. Bioanal. Chem.* **2008**, *391* (5), 1509–1519. https://doi.org/10.1007/s00216-008-1911-5.

(11) Hoummady, M.; Campitelli, A.; Wlodarski, W. Acoustic Wave Sensors: Design, Sensing Mechanisms and Applications. *Smart Mater. Struct.* **1999**, *6* (6), 647.

(12) Zhang, S. P.; Lata, J.; Chen, C.; Mai, J.; Guo, F.; Tian, Z.; Ren, L.; Mao, Z.; Huang, P. H.; Li, P.; Yang, S. J.; Huang, T. J. Digital Acoustofluidics Enables Contactless and Programmable Liquid Handling. *Nat. Commun.* **2018**, *9* (1), 2928-. https://doi.org/10.1038/s41467-018-05297-z.

(13) Liu, Y.; Li, Y.; el-Hady, A. M.; Zhao, C.; Du, J. F.; Liu, Y.; Fu, Y. Q. Flexible and Bendable Acoustofluidics Based on ZnO Film Coated Aluminium Foil. *Sensors Actuators B Chem.* **2015**, *221*, 230–235. https://doi.org/10.1016/J.SNB.2015.06.083.

(14) Xuan, W.; He, M.; Meng, N.; He, X.; Wang, W.; Chen, J.; Shi, T.; Hasan, T.; Xu, Z.; Yang, X. Fast Response and High Sensitivity ZnO/Glass Surface Acoustic Wave Humidity Sensors Using Graphene Oxide Sensing Layer. *Sci Rep* **2014**, *4*, 7206.

(15) Hu, J.; Odom, T. W.; Lieber, C. M. Chemistry and Physics in One Dimension: Synthesis and Properties of Nanowires and Nanotubes. *Acc. Chem. Res.* **1999**, *32* (5), 435–445. https://doi.org/10.1021/ar9700365.

(16) Zhong, L. W. Characterizing the Structure and Properties of Individual Wire-like Nanoentities. *Adv. Mater.* **2010**, *12* (17), 1295–1298.

(17) Qi, P.; Vermesh, O.; Grecu, M.; Javey, A.; Wang, Q.; Dai, H.; Peng, S.; Cho, K. J. Toward Large Arrays of Multiplex Functionalized Carbon Nanotube Sensors for Highly Sensitive and Selective Molecular Detection. *Nano Lett.* **2003**, *3* (3), 347–351. https://doi.org/10.1021/nl034010k.

(18) Lee, K. J.; Oh, H.; Jo, M.; Lee, K.; Yang, S. S. An Ultraviolet Sensor Using Spin–Coated ZnO Nanoparticles Based on Surface Acoustic Waves. *Microelectron. Eng.* **2013**, *111*, 105–109. https://doi.org/10.1016/J.MEE.2013.02.025.

(19) Jo, M.; Lee, K. J.; Yang, S. S. Sensitivity Improvement of the Surface Acoustic Wave Ultraviolet Sensor Based on Zinc Oxide Nanoparticle Layer with an Ultrathin Gold Layer. *Sensors Actuators A Phys.* **2014**, *210*, 59–66. https://doi.org/10.1016/J.SNA.2014.02.007.

(20) Wang, B.; Zhu, L. F.; Yang, Y. H.; Xu, N. S.; Yang, G. W. Fabrication of a SnO2 Nanowire Gas Sensor and Sensor Performance for Hydrogen. *J. Phys. Chem. C* **2008**, *112* (17), 6643–6647. https://doi.org/10.1021/jp8003147.

(21) Li, W.; Guo, Y. J.; Tang, Q. B.; Zu, X. T.; Ma, J. Y.; Wang, L.; Tao, K.; Torun, H.; Fu, Y. Q. Highly Sensitive Ultraviolet Sensor Based on ZnO Nanorod Film Deposited on ST-Cut Quartz Surface Acoustic Wave Devices. *Surf. Coatings Technol.* **2019**, *363*, 419–425. https://doi.org/10.1016/J.SURFCOAT.2019.02.041.

(22) Lupan, O.; Emelchenko, G. A.; Ursaki, V. V.; Chai, G.; Redkin, A. N.; Gruzintsev, A. N.; Tiginyanu, I. M.; Chow, L.; Ono, L. K.; Roldan Cuenya, B.; Heinrich, H; Yakimov, E. E. Synthesis and Characterization of ZnO Nanowires for Nanosensor Applications. *Mater. Res. Bull.* **2010**, *45* (8), 1026–1032. https://doi.org/10.1016/J.MATERRESBULL.2010.03.027.

(23) Idalia, B.; Markus, N. Microwave Chemistry for Inorganic Nanomaterials Synthesis. *Nanoscale* **2010**, *2* (8), 1358–1374.

(24) Patil, K. C.; Aruna, S. T.; Mimani, T. Combustion Synthesis: An Update. *Curr. Opin. Solid State Mater. Sci.* **2002**, *6* (6), 507–512. https://doi.org/10.1016/S1359-0286(02)00123-7.

(25) Mishra, Y. K.; Kaps, S.; Schuchardt, A.; Paulowicz, I.; Jin, X.; Gedamu, D.; Freitag, S.; Claus, M.; Wille, S.; Kovalev, A.; Gorb, S. N.; Adelung, R. Fabrication of Macroscopically Flexible and Highly Porous 3D Semiconductor Networks from Interpenetrating Nanostructures by a Simple Flame Transport Approach. *Part. Part. Syst. Charact.* **2013**, *30* (9), 775–783. https://doi.org/10.1002/ppsc.201300197.

(26) Mishra, Y. K.; Adelung, R. ZnO Tetrapod Materials for Functional Applications. *Mater. Today* **2018**, *21* (6), 631–651. https://doi.org/10.1016/J.MATTOD.2017.11.003.

(27) Mishra, Y. K.; Modi, G.; Cretu, V.; Postica, V.; Lupan, O.; Reimer, T.; Paulowicz, I.; Hrkac, V.; Benecke, W.; Kienle, L.; Adelung, R. Direct Growth of Freestanding ZnO Tetrapod Networks for Multifunctional Applications in Photocatalysis, UV Photodetection, and Gas Sensing. *ACS Appl. Mater. Interfaces* **2015**, *7* (26), 14303–14316. https://doi.org/10.1021/acsami.5b02816.

(28) Papavlassopoulos, H.; Mishra, Y. K.; Kaps, S.; Paulowicz, I.; Abdelaziz, R.; Elbahri, M.; Maser, E.; Adelung, R.; Röhl, C. Toxicity of Functional Nano-Micro Zinc Oxide Tetrapods: Impact of Cell Culture Conditions, Cellular Age and Material Properties. *PLoS One* **2014**, *9* (1), e84983. https://doi.org/10.1371/journal.pone.0084983.

(29) Chivukula, V.; Ciplys, D.; Shur, M.; Dutta, P. ZnO Nanoparticle Surface Acoustic Wave UV Sensor. *Appl. Phys. Lett.* **2010**, *96* (23), 233512. https://doi.org/10.1063/1.3447932.

(30) Sharma, M.; Joshi, M.; Nigam, S.; Shree, S.; Avasthi, D. K.; Adelung, R.; Srivastava, S. K.; Kumar Mishra, Y. ZnO Tetrapods and Activated Carbon Based Hybrid Composite: Adsorbents for Enhanced Decontamination of Hexavalent Chromium from Aqueous Solution. *Chem. Eng. J.* **2019**, *358*, 540–551. https://doi.org/10.1016/J.CEJ.2018.10.031.

(31) Kaps, S.; Bhowmick, S.; Gröttrup, J.; Hrkac, V.; Stauffer, D.; Guo, H.; Warren, O. L.; Adam, J.; Kienle, L.; Minor, A. M.; Adelung, R.; Mishra, Y. K. Piezoresistive Response of Quasi-One-Dimensional ZnO Nanowires Using an in Situ Electromechanical Device. *ACS Omega* **2017**, *2* (6), 2985–2993. https://doi.org/10.1021/acsomega.7b00041.

(32) Wang, B.-B.; Xie, J.-J.; Yuan, Q.; Zhao, Y.-P. Growth Mechanism and Joint Structure of ZnO Tetrapods. *J. Phys. D. Appl. Phys.* **2008**, *41* (10), 102005. https://doi.org/10.1088/0022-3727/41/10/102005.

(33) Ronning, C.; Shang, N. G.; Gerhards, I.; Hofsäss, H.; Seibt, M. Nucleation Mechanism of the Seed of Tetrapod ZnO Nanostructures. *J. Appl. Phys.* **2005**, *98* (3), 34307. https://doi.org/10.1063/1.1997290.

(34) Jin, H.; Tao, X.; Feng, B.; Yu, L.; Wang, D.; Dong, S.; Luo, J. A Humidity Sensor Based on Quartz Crystal Microbalance Using Graphene Oxide as a Sensitive Layer. *Vacuum* **2017**, *140*, 101–105.

(35) Lupan, O.; Chow, L.; Ono, L. K.; Cuenya, B. R.; Chai, G.; Khallaf, H.; Park, S.; Schulte, A. Synthesis and Characterization of Ag- or Sb-Doped ZnO Nanorods by a Facile Hydrothermal Route. *J. Phys. Chem. C* **2010**, *114* (29), 12401–12408. https://doi.org/10.1021/jp910263n.

(36) Chow, L.; Lupan, O.; Chai, G.; Khallaf, H.; Ono, L. K.; Roldan Cuenya, B.; Tiginyanu, I. M.; Ursaki, V. V.; Sontea, V.; Schulte, A. Synthesis and Characterization of Cu-Doped ZnO One-Dimensional Structures for Miniaturized Sensor Applications with Faster Response. *Sensors Actuators A Phys.* **2013**, *189*, 399–408. https://doi.org/10.1016/J.SNA.2012.09.006.

(37) Smith, W. R.; Gerard, H. M.; Collins, J. H.; Reeder, T. M.; Shaw, H. J. Analysis of Interdigital Surface Wave Transducers by Use of an Equivalent Circuit Model. *IEEE Trans. Microw. Theory Tech.* **1969**, *17* (11), 856–864.

(38) Bian, X.; Jin, H.; Wang, X.; Dong, S.; Chen, G.; Luo, J. K.; Deen, M. J.; Qi, B. UV Sensing Using Film Bulk Acoustic Resonators Based on Au/n-ZnO/Piezoelectric-ZnO/Al Structure. *Sci. Rep.* **2015**, *5*, 9123.

(39) Guo, Y. J.; Zhao, C.; Zhou, X. S.; Li, Y.; Zu, X. T.; Gibson, D.; Fu, Y. Q. Ultraviolet Sensing Based on Nanostructured ZnO/Si Surface Acoustic Wave Devices. *Smart Mater. Struct.* **2015**, *24* (12), 125015. https://doi.org/10.1088/0964-1726/24/12/125015.

(40) Chen, F.; Lee, K. J.; Lee, K.; Sang, S. Y. Low-Intensity Ultraviolet Detection Using a Surface Acoustic-Wave Sensor with a Ag-Doped ZnO Nanoparticle Film. *Smart Mater. Struct.* **2015**, *24* (1), 15010.

(41) Ballantine Jr, D. S.; White, R. M.; Martin, S. J.; Ricco, A. J.; Zellers, E. T.; Frye, G. C.; Wohltjen, H. *Acoustic Wave Sensors: Theory, Design and Physico-Chemical Applications*; Elsevier, 1996.

(42) Zhou, J.; Pang, H. F.; Garcia-Gancedo, L.; Iborra, E.; Clement, M.; Miguel-Ramos, M. De; Jin, H.; Luo, J. K.; Smith, S.; Dong, S. R. Discrete Microfluidics Based on Aluminum Nitride Surface Acoustic Wave Devices. *Microfluid. Nanofluidics* **2015**, *18* (4), 537–548.

(43) Bu, G.; Ciplys, D.; Shur, M.; Schowalter, L. J.; Schujman, S.; Gaska, R. Temperature Coefficient of SAW Frequency in Single Crystal Bulk AlN. *Electron. Lett.* **2003**, *39* (9), 755–757.

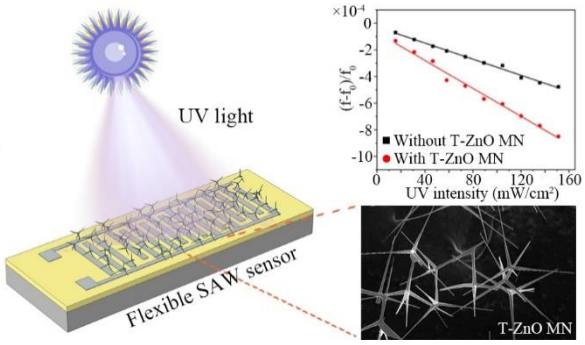

For Table of Contents Only